


Article

Evaluation of Drug-Loading Ability of Poly(Lactic Acid)/Hydroxyapatite Core–Shell Particles

Seiya Suzuki^{1,2}, Sungho Lee^{1,*} , Tatsuya Miyajima¹, Katsuya Kato¹ , Ayae Sugawara-Narutaki³ , Makoto Sakurai² and Fukue Nagata^{1,*} 

¹ National Institute of Advanced Industrial Science and Technology (AIST), 2266-98 Anagahora, Shimoshidami, Moriyama-ku, Nagoya 463-8560, Japan; seiya-suzuki@aist.go.jp (S.S.); t.miyajima@aist.go.jp (T.M.); katsuya-kato@aist.go.jp (K.K.)

² Department of Applied Chemistry, College of Engineering, Chubu University, Matsumoto-cho, Kasugai 487-8501, Japan; sakurai@isc.chubu.ac.jp

³ Department of Energy Engineering, Graduate School of Engineering, Nagoya University, Furo-cho, Chikusa-ku, Nagoya 464-8603, Japan; ayae@energy.nagoya-u.ac.jp

* Correspondence: sungho.lee@aist.go.jp (S.L.); f.nagata@aist.go.jp (F.N.); Tel.: +81-52-736-7387 (F.N.)

Abstract: Poly(lactic acid)/hydroxyapatite (PLA/HAp) core–shell particles are prepared using the emulsification method. These particles are safe for living organisms because they are composed of biodegradable polymers and biocompatible ceramics. These particles are approximately 50–100 nm in size, and their hydrophobic substance loading can be controlled. Hence, PLA/HAp core–shell particles are expected to be used as drug delivery carriers for hydrophobic drugs. In this work, PLA/HAp core–shell particles with a loading of vitamin K₁ were prepared, and their drug-loading ability was evaluated. The particles were 40–80 nm in diameter with a PLA core and a HAp shell. The particle size increased with an increase in the vitamin K₁ loading. The drug-loading capacity (LC) value of the particles, an indicator of their drug-loading ability, was approximately 250%, which is higher than the previously reported values. The amount of vitamin K₁ released from the particles increased as the pH of the soaking solution decreased because the HAp shell easily dissolved under the acidic conditions. The PLA/HAp particles prepared in this work were found to be promising candidates for drug delivery carriers because of their excellent drug-loading ability and pH sensitivity.

Keywords: hydroxyapatite; poly(lactic acid); drug delivery system; loading capacity; core–shell particles



Citation: Suzuki, S.; Lee, S.; Miyajima, T.; Kato, K.; Sugawara-Narutaki, A.; Sakurai, M.; Nagata, F. Evaluation of Drug-Loading Ability of Poly(Lactic Acid)/Hydroxyapatite Core–Shell Particles. *Materials* **2021**, *14*, 1959. <https://doi.org/10.3390/ma14081959>

Academic Editor: Albena Lederer

Received: 26 February 2021

Accepted: 12 April 2021

Published: 14 April 2021

Publisher's Note: MDPI stays neutral with regard to jurisdictional claims in published maps and institutional affiliations.



Copyright: © 2021 by the authors. Licensee MDPI, Basel, Switzerland. This article is an open access article distributed under the terms and conditions of the Creative Commons Attribution (CC BY) license (<https://creativecommons.org/licenses/by/4.0/>).

1. Introduction

Carriers that form part of drug delivery systems (DDS carriers) have attracted considerable attention [1]. DDS carriers are expected to deliver drugs to the appropriate sites in living organisms effectively and safely. In addition, the components of the DDS carriers should not remain in the body. Several materials, such as phospholipids, polyethylene glycol (PEG), and biodegradable polymers, have been used as DDS carriers. Phospholipids are liposomes composed of bilayer membranes [2]. The liposome is hydrophilic inside and has a hydrophobic membrane on the outside. PEG is a polymeric micelle composed of biocompatible molecules [3]. Polymeric micelles are formed from hydrophilic and hydrophobic polymers by the self-association of block copolymers. The degradation rate of microspheres with biodegradable polymers, such as poly(lactic acid) (PLA) and poly(lactic glycolic acid) (PLGA), can reportedly be controlled in vivo by adjusting their composition [4–9]. PLGA microspheres loaded with superparamagnetic iron oxide nanoparticles and dexamethasone acetate have been reported for the treatment of local inflammatory diseases [7]. PLGA microspheres/poly(vinyl alcohol) (PVA) hydrogel composites with dexamethasone and vascular endothelial growth factor have been reported to stimulate angiogenesis [8]. Inflamed areas exhibit greater vascular permeability and leakage of larger

molecules than normal areas [10]; this is known as the enhanced permeability and retention effect (EPR effect) [11,12]. Nano-sized DDS carriers (20–200 nm) were designed to passively target inflammatory sites, which have interendothelial pores in the blood vessels [13]. Doxorubicin (DOX)-loaded liposomal preparations have been approved for the treatment of cancers such as Kaposi's sarcoma using the EPR effect [14].

Hydroxyapatite ($\text{Ca}_{10}(\text{PO}_4)_6(\text{OH})_2$ or HAp), a well-known bioceramic, is an inorganic component of bone. HAp exhibits excellent biocompatibility and bioresorbability [15]. Thus, various DDS carriers using HAp have been reported [16–20]. Tetracycline hydrochloride, an antibiotic, loaded onto porous HAp was composited with polycaprolactone, and the drug-release behavior of the composite was controlled by varying the mixing ratio [16]. Nanocomposites of DOX-loaded HAp and folic acid have shown enhanced drug effects on tumors [19].

Seventy percent of novel drugs are hydrophobic and the number of these drugs continues to increase [21]. Thus, the ability to load hydrophobic substances is a great advantage for DDS carriers. DDS carriers may reduce the burden on patients by decreasing the frequency of drug administration. However, carriers must have a large drug-loading capacity with a controlled release. Hence, improvements in the drug-loading capacity of DDS carriers have been studied [22,23]. Polymeric micelles have been developed to improve the drug-loading capacity via π - π stacking interactions [22] and by inducing additional π - π interactions [23]. The drug-loading capacity values of polymeric micelles with π - π stacking interactions and additional π - π interactions are 18% and 16%, respectively, which are larger than those of other poly(ϵ -caprolactone) and poly(L-lactide) polymer micelles (3–5%) [24]. Carbon dot particles can absorb drugs on their surfaces with a drug-loading capacity range of 310–439% [25]. Core-shell particles are normally composed of a core encapsulated within a shell, and the shell is expected to inhibit the reactivity and solubility of the materials loaded in the core. DOX-loaded poly(ethylene oxide)-poly(propylene oxide)-poly(ethylene oxide) block copolymers have been reported to be useful for multidrug-resistant cancer cells [26]. DOX-loaded Fe_3O_4 /mesoporous nano-silica core-shell particles with a drug-loading capacity of 20% exhibit a suppression effect on the degradation and elution of DOX as compared to the administration of free DOX [27].

PLA particles for application as DDS carriers can be prepared using the emulsion method. However, it is necessary to use surfactants to stabilize the interface of these particles [28]. Moreover, a large amount of surfactants is required to prepare small particles [29]. Most surfactants are nonbiodegradable and tend to remain in the resulting particles [29]. In our previous work, we prepared PLA/HAp core-shell particles using the emulsification method without involving any surfactant [30–32]. The surface of PLA was stabilized with calcium ions, which bonded with the carboxyl groups in PLA [33]. Subsequently, HAp precipitated on the carboxyl groups, which bonded with the calcium ions; thus, the HAp shell was formed after aging for a certain duration [30,31]. Hydrophobic substances could be easily encapsulated within the PLA micelles of PLA/HAp core-shell particles. The particles were found to be safe for living organisms because they were composed of PLA and HAp. The particles were 40–100 nm in size and were expected to show the EPR effect on tumors and inflammatory sites. The present work represents a fundamental study of the drug-loading ability of PLA/HAp core-shell particles for application as DDS carriers. Vitamin K_1 was chosen as the model drug for the evaluation of drug-loading capacity as it is a liquid fat-soluble vitamin. Vitamin K_1 -loaded PLA/HAp core-shell particles were prepared and their drug-loading capacity and drug-release behavior in phosphate buffer solutions were investigated.

2. Materials and Methods

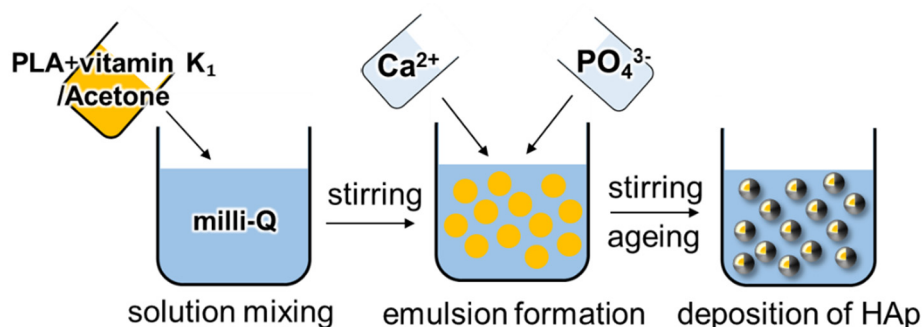
2.1. Materials

Acetone (99.5%, Wako Pure Chemical Industries, Osaka, Japan), vitamin K_1 (97%, Wako Pure Chemical Industries), $\text{Ca}(\text{CH}_3\text{COO})_2 \cdot \text{H}_2\text{O}$ (99%, Wako Pure Chemical Industries), $(\text{NH}_4)_2\text{HPO}_4$ (99%, Wako Pure Chemical Industries), PLA ($(\text{C}_6\text{H}_8\text{O}_4)_n$, Mw

10–18 kDa, Sigma-Aldrich, St. Louis, Missouri, United States), and ultrapure water (milli-Q, resistivity > 18.2 M Ω ·cm) were used to prepare the PLA/HAp core-shell particles. A phosphate buffer solution was prepared using Na₂HPO₄ (99%, Wako Pure Chemical Industries) and KH₂PO₄ (99.5%, Wako Pure Chemical Industries) for drug-release testing.

2.2. Preparation of Vitamin K₁-Loaded PLA/HAp Core-Shell Particles

Vitamin K₁-loaded PLA/HAp core-shell particles were prepared using an emulsification method (Scheme 1). The details of the preparation of the PLA/HAp core-shell particles are described in our previous paper [30–32]. In brief, PLA (20 mg) and various amounts of vitamin K₁ (0, 50, 100, and 200 mg) were dissolved in 4 mL of acetone (denoted as PLHA-V_x, where *x* is the amount of vitamin K₁, (*x* = 0, 50, 100, 200)). This solution was then added to 160 mL of ultrapure water. To the resulting mixture, 20 mL of a 20 mM calcium acetate solution and 20 mL of a 12 mM potassium phosphate solution were added under stirring at 25 °C. The resulting solutions were aged for three days. The pH of the solutions was measured before and 1 h after the addition of the phosphate ions and after aging for 72 h (Table 1). The aged solutions were centrifuged (6000 rpm, 10 min). The supernatant was removed, and the particles were washed with ultrapure water. The particles were resuspended in 20 mL of ultrapure water. The residual vitamin K₁ in the container was collected by dissolving it in ethanol, and its concentration was measured using ultraviolet-visible absorption spectroscopy (UV-Vis; JASCO Corporation, V-750) over the wavelength range of 200–900 nm (bandwidth: 2.0 nm; scanning speed: 400 nm/min). The absorption spectrum of vitamin K₁ was set to 273 nm.



Scheme 1. Preparation of the vitamin K₁-loaded PLA/HAp core-shell particle solutions.

Table 1. pH values of the PLHA-V_x solutions under different conditions.

Sample Code	Addition of Phosphate Ion		After Aging (72 h)
	Before	1 h after	
PLHA-V0	7.61	6.81	6.19
PLHA-V50	7.67	6.86	6.23
PLHA-V100	7.61	6.80	6.13
PLHA-V200	7.70	6.88	6.35

2.3. Characterization of the Vitamin K₁-Loaded PLA/HAp Core-Shell Particles

The crystalline phase of PLHA-V_x was evaluated using X-ray diffraction (XRD; Rigaku, Tokyo, Japan). The XRD conditions were as follows: CuK α radiation (40 kV, 30 mA); 1.0 °/min, and a 2 θ range of 3–60°. PLHA-V_x was evaluated by the attenuated total reflection (ATR) method using a Fourier transform infrared spectrometer (FT-IR; JASCO Corporation, Tokyo, Japan) in the range of 400–4000 cm^{−1}. The morphology of PLHA-V_x was observed using field emission scanning electron microscopy (FE-SEM; Hitachi, Tokyo, Japan). The PLHA-V_x-containing solutions were dropped onto an aluminum sample stage and dried gently at 37 °C. Subsequently, PLHA-V_x was coated with a layer of amorphous osmium (Meiwafosis, Tokyo, Japan). The diameters of the PLHA-V_x particles

were measured using a laser diffraction particle size analyzer (SALD-7500nano, Shimadzu, Kyoto, Japan). Particles weighing 5 mg were dispersed in 100 mL of ultrapure water and sonicated during the measurement. The PLHA-V0 solution was directly dropped onto a carbon grid and dried. The samples were observed using transmission electron microscopy (TEM; JEOL, Tokyo, Japan). The organic/inorganic ratio of PLHA-V x was evaluated using thermogravimetry–differential thermal analysis (TG–DTA; Rigaku, Tokyo, Japan). PLHA-V x (5 mg) was used for the analysis, and the same amount of Al₂O₃ was used as the reference. TG–DTA was performed at room temperature (approximately 25 °C) to 1000 °C (2 °C/min) under air flow (200 mL/min). For the XRD, FT-IR, and TG–DTA measurements, freeze-dried particles were used.

2.4. Drug-Release Test of the Vitamin K₁-Loaded PLA/HAp Core–Shell Particles

PLHA-V200 was chosen for the drug-release test because it contained the highest amount of drug among all the PLHA-V x samples investigated. PLHA-V200 was added to phosphate buffer solutions with the pH values of 4.5, 5.5, and 7.4, and 1.88 mg of PLHA-V200 was soaked in 1 mL of the buffer solutions. The solutions were maintained at 37 °C for 1–6 days and stirred during the release test to prevent particle agglomeration. The phosphate buffer solutions (pH 4.5, 5.5, and 7.4) were prepared by mixing 66 mM Na₂HPO₄ and KH₂PO₄ in the Na₂HPO₄:KH₂PO₄ ratios of 0:20, 1:19, and 16:4 at pH = 4.5, 5.5, and 7.4, respectively. In this work, a protein-free phosphate buffer solution was selected for the drug-release test to investigate the fundamental properties of the PLA/HAp particles. The supernatant of the solution was collected by centrifugation (14,000 rpm) and subjected to Ultraviolet Visible Absorption Spectroscopy analysis (UV–Vis, JASCO Corporation, Tokyo, Japan).

3. Results

During the particle preparation, the pH of the PLHA-V x solutions decreased after the addition of the phosphate ions (Table 1), indicating the precipitation of calcium phosphate. It is known that the pH decreases with precipitation of HAp [34]. The XRD patterns of PLHA-V x are shown in Figure 1a. PLHA-V x exhibited intense peaks at $2\theta = 26^\circ$ and 32° , corresponding to the 002 and 211 planes of HAp (JCPDS: 09-432), respectively. In addition, a halo peak at around $2\theta = 18^\circ$ was observed for PLHA-V50, -V100, and -V200. The FT-IR spectra of the particles are shown in Figure 1b. The bands corresponding to the phosphate group of HAp were the ν_2 bending vibration at 469 cm⁻¹; the ν_4 bending vibration at 560, 602, and 623 cm⁻¹; the ν_1 symmetric stretching vibration at 959 cm⁻¹; and the ν_3 asymmetric stretching vibration at 1024 cm⁻¹ [35–37]. The carboxyl group of PLA was assigned to the band at 858 cm⁻¹ for the –C–COO stretching vibration, 1078 cm⁻¹ for the COC symmetric stretching vibration, 1179 cm⁻¹ for the COC asymmetric stretching vibration and CH₃ asymmetric bending vibration, and 1746 cm⁻¹ for the C=O stretching vibration [38]. In addition, the vitamin K₁ bands of PLHA-V50, -V100, and -V200 were located at 1296 and 1328 cm⁻¹ for the –C=C and C–C groups, 1374 cm⁻¹ for the CH₃ group, 1457 cm⁻¹ for the CH₂ group, 1593 and 1615 cm⁻¹ for the C=C group, and 1657 cm⁻¹ for the C=O group [39].

The PLHA-V x particles were spherical, as shown in the SEM images in Figure 2. The particle size distribution is shown in Figure 3. The average particle sizes of PLHA-V0, -V50, -V100, and -V200 were 27, 47, 104, and 105 nm, respectively. The particle size was increased with an increasing drug-loading amount. The TEM image of PLHA-V0 is shown in Figure 4. The inner gray sphere and black shell were approximately 40 nm in diameter and 6 nm in thickness, respectively. The percentages of the organic/inorganic components in PLHA-V x were estimated using TG–DTA (Table 1), where the inorganic component of PLHA-V x was HAp, and the organic component was the sum of PLA and vitamin K₁. The amount of residual vitamin K₁ in the container for the preparation of PLHA-V200 was measured to be 109 mg using UV–Vis spectroscopy. The loading amount of vitamin K₁ in PLHA-V200 was calculated to be 91 mg.

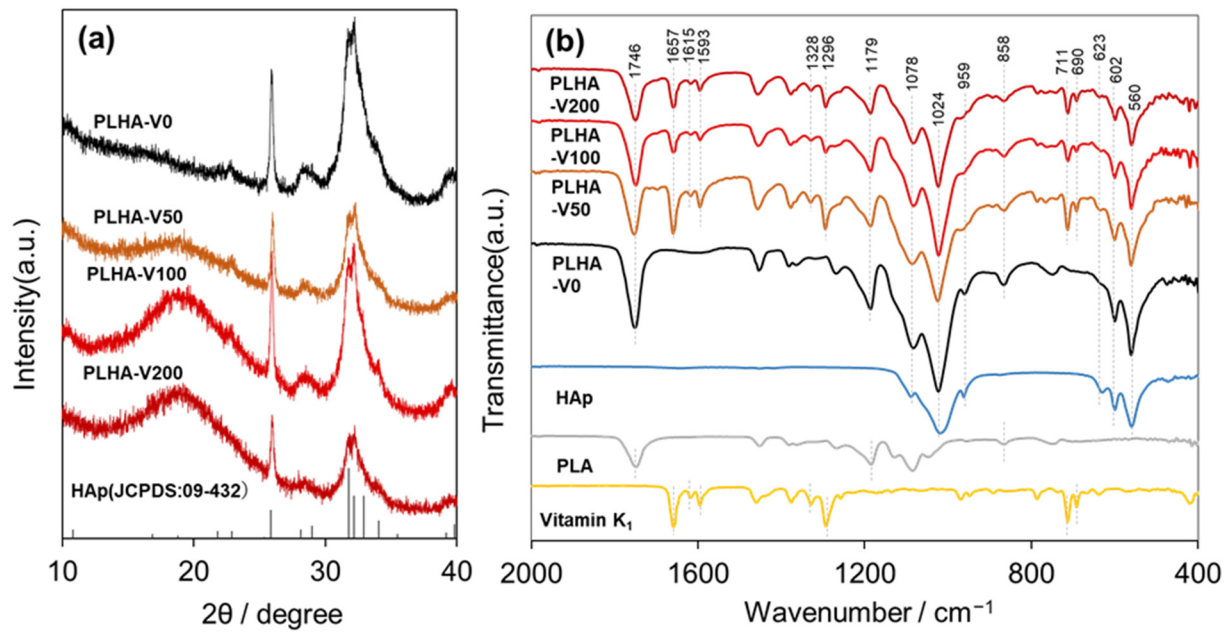


Figure 1. (a) X-ray diffraction (XRD) patterns and (b) Fourier transform infrared (FT-IR) spectra for the PLHA-V_x particles.

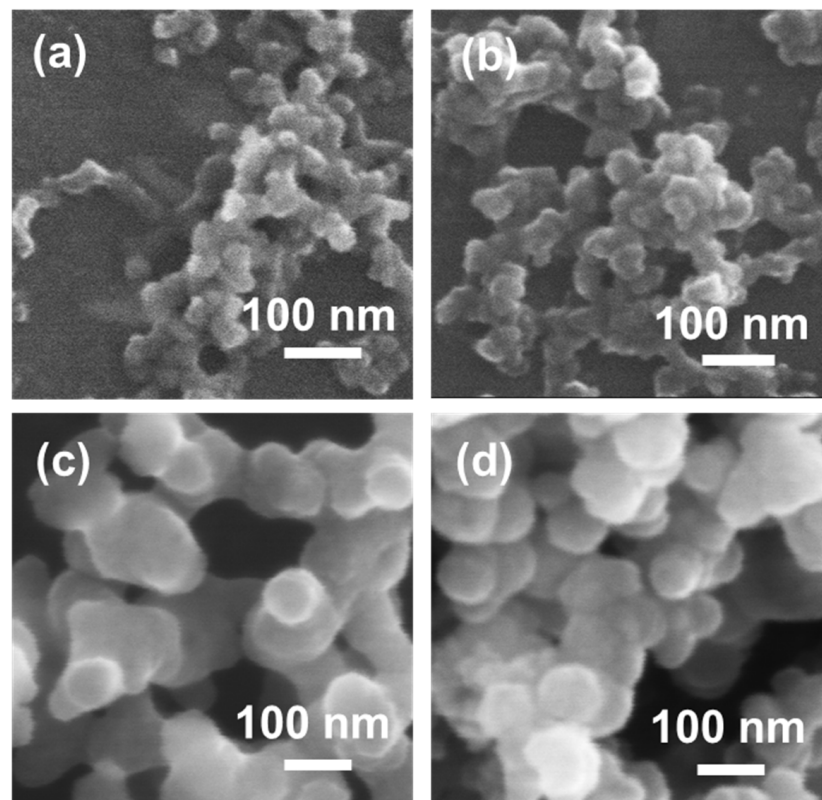


Figure 2. Scanning electron microscopy (SEM) images of (a) PLHA-V0, (b) PLHA-V50, (c) PLHA-V100, and (d) PLHA-V200.

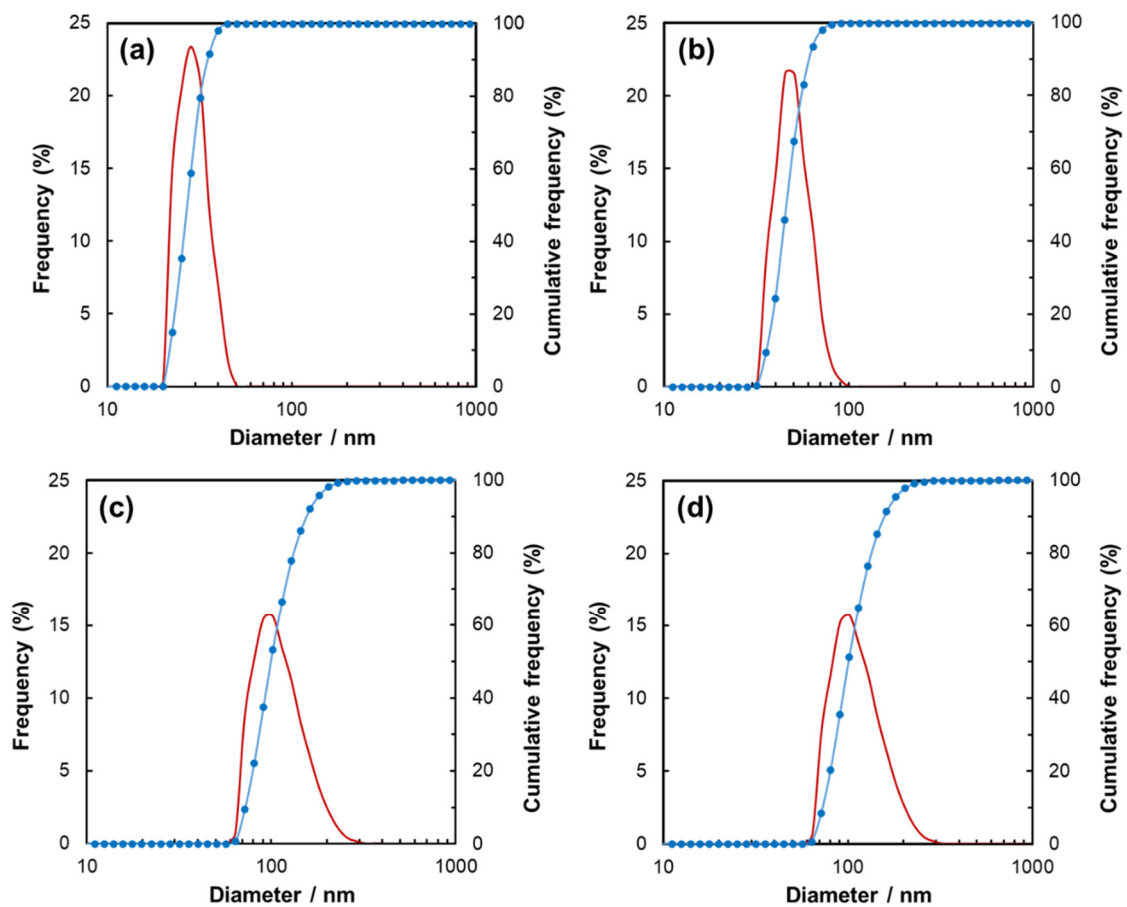


Figure 3. Particle diameter distribution of (a) PLHA-V0, (b) PLHA-V50, (c) PLHA-V100, and (d) PLHA-V200. Red solid lines represent the appearance frequency, and blue solid lines represent the cumulative frequency.

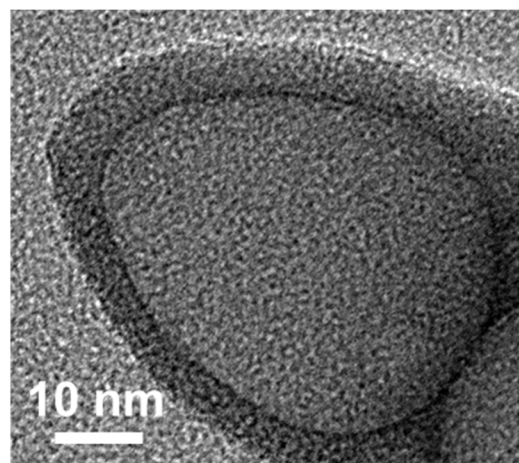


Figure 4. TEM image of PLHA-V0.

The vitamin K₁-releasing behavior of PLHA-V200 in the phosphate buffer at various pH levels is shown in Figure 5. PLHA-V200 was chosen for the release test because it contained the largest amount of vitamin K₁ among all the PLHA-V_x samples investigated. Vitamin K₁ was not found to undergo the initial burst release behavior in PLHA-V200 at all pH levels. The amount of vitamin K₁ released in the phosphate buffer at pH 4.5, 5.6, and 7.4, was 18, 13, and 5 µg, respectively, and this amount increased as the pH of the phosphate buffer solution decreased.

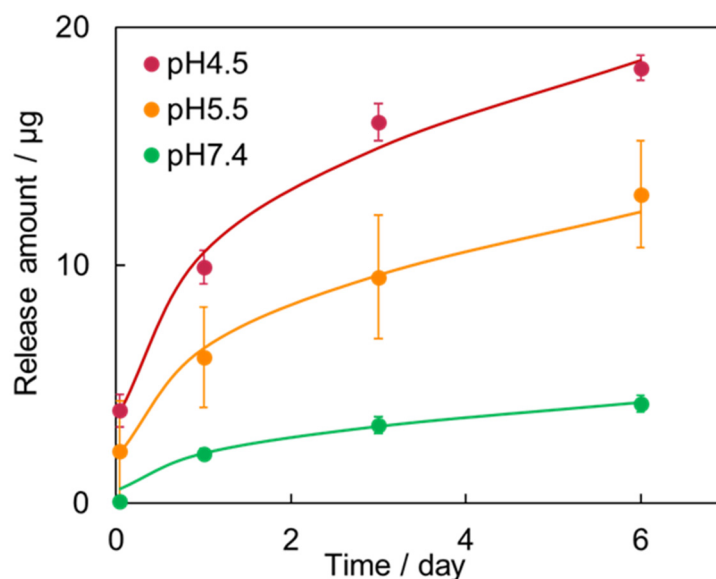


Figure 5. Vitamin K₁-releasing behavior of PLHA-V200 in phosphate buffer at various pH levels. Error bars represent the standard deviation ($n = 3$). Solid lines represent Korsmeyer–Peppas fitted release profiles.

4. Discussion

The XRD patterns of the PLHA-V x particles showed peaks corresponding to HAp. PLHA-V50, -V100, and -V200 showed a halo peak centered at $2\theta = 18^\circ$, which may have originated from vitamin K₁. The intensity of this peak increased with an increase in the vitamin K₁ content. This peak was confirmed for a mixture of PLHA-V0 and vitamin K₁ (Figure S1 in Supplementary Materials). In addition, the XRD peaks of PLHA-V x were not sharp, which were similar to those of biological HAp [40,41]. The FT-IR spectra of PLHA-V x showed bands corresponding to the phosphate and carboxyl groups of HAp and PLA, respectively. The bands corresponding to vitamin K₁ were observed in the spectra of PLHA-V50, -V100, and -V200, whereas these bands were not observed for PLHA-V0. The hierarchical architecture of PLHA-V0 was composed of a PLA core and a HAp shell, as shown in the TEM image. Additionally, the PLHA-V x particles were spherical in shape, as confirmed by the SEM images, and no other precipitation was visible. Thus, PLHA-V x was successfully prepared as a core-shell structure by loading vitamin K₁.

The diameters of the PLHA-V0, -V50, -V100, and -V200 particles were 27, 47, 104, and 105 nm, respectively, and the size of particles increased with an increase in the amount of vitamin K₁. Additionally, the organic component of PLHA-V x increased with the increasing amounts of vitamin K₁. Hence, the particles expanded with an increase in the amount of drug that was encapsulated.

The loading capacity (LC) of DDS carriers is an indicator of their drug-loading ability and can be calculated using the following equation [25,42,43]:

$$LC (\%) = \frac{W_d}{W_c} \times 100 \quad (1)$$

where W_d is the mass of the drug (mg) and W_c is the mass of the DDS carriers (mg). In this work, the LC can be altered as follows.

$$LC (\%) = \frac{R_V}{R_H + R_P} \times 100 \quad (2)$$

where R_V , R_H , and R_P are the weight ratios of vitamin K₁, HAp, and PLA in the particles, respectively. The R_H and $(R_V + R_P)$ ratios were obtained using TG–DTA (Table 2). In the case of PLHA-V200, the R_V can be altered as follows:

$$R_V = 84.5 - R_P \quad (3)$$

where R_H is 15.5, as determined from the TG–DTA results. The weight ratio of R_V and R_P can be obtained as follows:

$$R_V : R_P = W_V : W_P \quad (4)$$

where W_V and W_P are the weights of vitamin K₁ and PLA (mg) in PLHA-V200, respectively. W_P is the amount of PLA used for particle preparation, which was 20 mg. W_V is the amount of vitamin K₁ loaded into PLHA-V200, as obtained from the UV–Vis spectrum, which was 109 mg. $R_V:R_P$ can be calculated as 71.4:13.1, from the values of W_V and W_P above. The weight ratio of HAp, PLA, and vitamin K₁ in PLHA-V200 is 15.5, 13.1, and 71.4%, respectively. Consequently, the LC value of PLHA-V200 was calculated to be 250%. Zhang et al. reported that polymeric micelles with anticancer agents, which were prepared by exploiting the π – π interactions between biodegradable polymers and disulfide bonds, exhibited an LC value of 18% [22]. Li et al. reported that polymeric micelles with π – π conjugated moieties as lipophilic segments for delivering anticancer agents exhibited an LC value of 15% [23]. Al-Amin et al. reported liposome particles with an LC value of 12% [44]. Therefore, PLHA-V x exhibited an excellent drug-loading capacity, with an LC value of 250%.

Table 2. Organic/inorganic percentage of PLHA-V x .

Sample	HAp (%)	Organic Component (%)
PLHA-V0	50.3	49.7
PLHA-V50	27.8	72.2
PLHA-V100	24.9	75.1
PLHA-V200	15.5	84.5

The amount of vitamin K₁ released from the particles increased as the pH of the phosphate buffer solution decreased. HAp is poorly soluble under neutral and basic conditions [45] and readily dissolves under acidic conditions. Thus, the HAp shell can easily dissolve at pH 4.5, and therefore, a larger amount of vitamin K₁ was released compared with that at pH 7.4. Furthermore, PLHA-V x showed no initial burst release behavior, and vitamin K₁ was released gradually during immersion. The release behavior of PLHA-V200 showed good correlation with the Korsmeyer–Peppas equation in pH 4.5, 5.5, and 7.4 ($R^2 > 0.95$) [46]. These results suggest that PLA/HAp core–shell particles are excellent candidates for DDS carriers with a larger drug-loading capacity and pH sensitivity.

5. Conclusions

PLHA-V x was prepared, and its drug-loading ability was evaluated. PLHA-V x was composed of PLA and HAp and was spherical in shape with a diameter of 40–80 nm. The diameter of PLHA-V x increased with an increase in the amount of vitamin K₁. Thus, vitamin K₁ was successfully encapsulated in the PLA/HAp particles. The LC value of PLHA-V200 was 250%, which is larger than those reported previously. PLHA-V200 showed pH sensitivity and no initial burst release behavior. Thus, PLHA-V x is a potential candidate for DDS carriers because of its excellent drug-loading ability and pH sensitivity.

Supplementary Materials: The following are available online at <https://www.mdpi.com/article/10.3390/ma14081959/s1>, Figure S1: XRD patterns of PLHA-V0 and PLHA-V0 + vitamin K₁ mixture.

Author Contributions: Conceptualization, S.L., T.M., K.K., A.S.-N., M.S. and F.N.: methodology; S.S., S.L., K.K. and F.N.: validation; S.S., S.L., T.M., K.K., A.S.-N. and F.N.: formal analysis; S.S., S.L. and F.N.: investigation; S.S., S.L. and F.N.: resources; S.S., S.L. and F.N.: data curation; S.S., S.L. and F.N.: writing—original draft preparation; S.S., S.L. and F.N.: writing—review and editing; S.L. T.M., K.K., A.S.-N., M.S. and F.N.: visualization; S.S., S.L. and F.N.: supervision; S.L. and F.N.: project administration; and F.N.: funding acquisition. All authors have read and agreed to the published version of the manuscript.

Funding: This work was supported by JST A-STEP Grant Number JPMJTS1624 and AMED under Grant Number JP20he0622038.

Institutional Review Board Statement: Not applicable.

Informed Consent Statement: Not applicable.

Data Availability Statement: Data sharing is not applicable to this article.

Acknowledgments: The authors acknowledge T. Matsubara (Nagoya Institute of Technology) for providing TEM analysis of the nanoparticles.

Conflicts of Interest: The authors declare no conflict of interest.

References

1. Ju, Y.; Guo, H.; Edman, M.; Hamm-Alvarez, S.F. Application of advances in endocytosis and membrane trafficking to drug delivery. *Adv. Drug Del. Rev.* **2020**, *157*, 118–141. [[CrossRef](#)]
2. Blume, G.; Cevc, G. Liposomes for the sustained drug release in vivo. *Biochim. Biophys. Acta* **1990**, *1029*, 91–97. [[CrossRef](#)]
3. Nagasaki, Y.; Okada, T.; Scholz, C.; Iijima, M.; Kato, M.; Kataoka, K. The Reactive Polymeric Micelle Based on An Aldehyde-Ended Poly(ethylene glycol)/Poly(lactide) Block Copolymer. *Macromolecules* **1998**, *31*, 1473–1479. [[CrossRef](#)]
4. Peltonen, L.; Aitta, J.; Hyvönen, S.; Karjalainen, M.; Hirvonen, J. Improved entrapment efficiency of hydrophilic drug substance during nanoprecipitation of poly (l) lactide nanoparticles. *AAPS PharmSciTech* **2009**, *5*, 115. [[CrossRef](#)]
5. Ogawa, Y.; Okada, H.; Yamamoto, Y.; Shimamoto, T. In Vivo Release Profiles of Leuprolide Acetate from Microcapsules Prepared with Poly(lactic Acids or Copoly (Lactic/Glycolic) Acids and In Vivo Degradation of These Polymers. *Chem. Pharm. Bull.* **1988**, *36*, 2576–2581. [[CrossRef](#)] [[PubMed](#)]
6. Nagai, Y.; Lee, J.J.; Yamane, H. Hydrolytic degradation of low molecular weigh poly(lactic acid)s and their drug eluting behavior. *J. Soc. Mater. Sci. Jpn.* **2011**, *60*, 2–7. [[CrossRef](#)]
7. Fredenberg, S.; Wahlgren, M.; Reslow, M.; Axelsson, A. The mechanisms of drug release in poly(lactic-co-glycolic acid)-based drug delivery systems—A review. *Int. J. Pharm.* **2011**, *415*, 34–52. [[CrossRef](#)]
8. Butoescu, N.; Seemayer, C.A.; Foti, M.; Jordan, O.; Doelker, E. Dexamethasone-containing PLGA superparamagnetic microparticles as carriers for the local treatment of arthritis. *Biomaterials* **2009**, *30*, 1772–1780. [[CrossRef](#)]
9. Patil, S.D.; Papadimitrakopoulos, F.; Burgess, D.J. Concurrent delivery of dexamethasone and VEGF for localized inflammation control and angiogenesis. *J. Control. Release* **2007**, *117*, 68–79. [[CrossRef](#)]
10. Torchilin, V. Tumor delivery of macromolecular drugs based on the EPR effect. *Adv. Drug Del. Rev.* **2011**, *63*, 131–135. [[CrossRef](#)]
11. Matsumura, Y.; Maeda, H. A new concept for macromolecular therapeutics in cancer chemotherapy: Mechanism of tumortropic accumulation of proteins and the antitumor agent smancs. *Cancer Res.* **1986**, *46*, 6387. [[PubMed](#)]
12. Maeda, H. SMANCS and polymer-conjugated macromolecular drugs: Advantages in cancer chemotherapy. *Adv. Drug Del. Rev.* **1991**, *6*, 181–202. [[CrossRef](#)]
13. Hollis, C.P.; Weiss, H.L.; Leggas, M.; Evers, B.M.; Gemeinhart, R.A.; Li, T. Biodistribution and bioimaging studies of hybrid paclitaxel nanocrystals: Lessons learned of the EPR effect and image-guided drug delivery. *J. Control. Release* **2013**, *172*, 12–21. [[CrossRef](#)] [[PubMed](#)]
14. Fang, J.; Nakamura, H.; Maeda, H. The EPR effect: Unique features of tumor blood vessels for drug delivery, factors involved, and limitations and augmentation of the effect. *Adv. Drug Del. Rev.* **2011**, *63*, 136–151. [[CrossRef](#)] [[PubMed](#)]
15. Oyane, A.; Tsurushima, H.; Sogo, Y.; Ito, A.; Mutsuzaki, H. Development of apatite based biomaterials utilizing, biologically functional molecules. *New Glass* **2009**, *24*, 35–42.
16. Kim, H.-W.; Knowles, J.C.; Kim, H.-E. Hydroxyapatite/poly(ϵ -caprolactone) composite coatings on hydroxyapatite porous bone scaffold for drug delivery. *Biomaterials* **2004**, *25*, 1279–1287. [[CrossRef](#)]
17. dos Apostolos, R.C.R.; Andrade, G.F.; da Silva, W.M.; de Assis Gomes, D.; de Miranda, M.C.; de Sousa, E.M.B. Hybrid polymeric systems of mesoporous silica/hydroxyapatite nanoparticles applied as antitumor drug delivery platform. *Int. J. Appl. Ceram. Technol.* **2019**, *16*, 1836–1849. [[CrossRef](#)]
18. Kundu, B.; Ghosh, D.; Sinha, M.K.; Sen, P.S.; Balla, V.K.; Das, N.; Basu, D. Doxorubicin-intercalated nano-hydroxyapatite drug-delivery system for liver cancer: An animal model. *Ceram. Int.* **2013**, *39*, 9557–9566. [[CrossRef](#)]
19. Sun, W.; Fan, J.L.; Wang, S.Z.; Kang, Y.; Du, J.J.; Peng, X.J. Biodegradable Drug-Loaded Hydroxyapatite Nanotherapeutic Agent for Targeted Drug Release in Tumors. *ACS Appl. Mater. Interfaces* **2018**, *10*, 7832–7840. [[CrossRef](#)]

20. Verma, G.; Shetake, N.G.; Pandrekar, S.; Pandey, B.N.; Hassan, P.A.; Priyadarsini, K.I. Development of surface functionalized hydroxyapatite nanoparticles for enhanced specificity towards tumor cells. *Eur. J. Pharm. Sci.* **2020**, *144*, 105206. [[CrossRef](#)] [[PubMed](#)]
21. Kawabata, Y.; Wada, K.; Nakatani, M.; Yamada, S.; Onoue, S. Formulation design for poorly water-soluble drugs based on biopharmaceutics classification system: Basic approaches and practical applications. *Int. J. Pharm.* **2011**, *420*, 1–10. [[CrossRef](#)] [[PubMed](#)]
22. Zhang, H.; Yan, J.; Mei, H.; Cai, S.; Li, S.; Cheng, F.; Cao, J.; He, B. High-drug-loading capacity of redox-activated biodegradable nanoplatform for active targeted delivery of chemotherapeutic drugs. *Regen. Biomater.* **2020**, *7*, 359–369. [[CrossRef](#)] [[PubMed](#)]
23. Li, Y.; Su, T.; Li, S.; Lai, Y.; He, B.; Gu, Z. Polymeric micelles with π - π conjugated moiety on glycerol dendrimer as lipophilic segments for anticancer drug delivery. *Biomater. Sci.* **2014**, *2*, 775–783. [[CrossRef](#)]
24. Cheng, F.; Guan, X.; Cao, H.; Su, T.; Cao, J.; Chen, Y.; Cai, M.; He, B.; Gu, Z.; Luo, X. Characteristic of core materials in polymeric micelles effect on their micellar properties studied by experimental and dpd simulation methods. *Int. J. Pharm.* **2015**, *492*, 152–160. [[CrossRef](#)]
25. Peng, Z.; Li, S.; Han, X.; Al-Youbi, A.O.; Bashammakh, A.S.; El-Shahawi, M.S.; Leblanc, R.M. Determination of the composition, encapsulation efficiency and loading capacity in protein drug delivery systems using circular dichroism spectroscopy. *Anal. Chim. Acta* **2016**, *937*, 113–118. [[CrossRef](#)] [[PubMed](#)]
26. Batrakova, E.V.; Dorodnych, T.Y.; Klinskii, E.Y.; Kliushnenkova, E.N.; Shemchukova, O.B.; Goncharova, O.N.; Arjakov, S.A.; Alakhov, V.Y.; Kabanov, A.V. Anthracycline antibiotics non-covalently incorporated into the block copolymer micelles: In vivo evaluation of anti-cancer activity. *Br. J. Cancer* **1996**, *74*, 1545–1552. [[CrossRef](#)] [[PubMed](#)]
27. Chen, Y.; Chen, H.; Zeng, D.; Tian, Y.; Chen, F.; Feng, J.; Shi, J. Core/Shell Structured Hollow Mesoporous Nanocapsules: A Potential Platform for Simultaneous Cell Imaging and Anticancer Drug Delivery. *ACS Nano* **2010**, *4*, 6001–6013. [[CrossRef](#)]
28. Danhier, F.; Ansorena, E.; Silva, J.M.; Coco, R.; Le Breton, A.; Préat, V. PLGA-based nanoparticles: An overview of biomedical applications. *J. Control. Release* **2012**, *161*, 505–522. [[CrossRef](#)]
29. Rao, J.P.; Geckeler, K.E. Polymer nanoparticles: Preparation techniques and size-control parameters. *Prog. Polym. Sci.* **2011**, *36*, 887–913. [[CrossRef](#)]
30. Nagata, F.; Miyajima, T.; Kato, K. Preparation of phylloquinone-loaded poly(lactic acid)/hydroxyapatite core-shell particles and their drug release behavior. *Adv. Powder Technol.* **2016**, *27*, 903–907. [[CrossRef](#)]
31. Hanasaki, M.; Nagata, F.; Miyajima, T.; Kato, K. Controlling particle size of poly(lactic acid)/hydroxyapatite nanoparticles. *Trans. Mat. Res. Soc. Jpn.* **2018**, *43*, 135–138. [[CrossRef](#)]
32. Lee, S.; Miyajima, T.; Sugawara-Narutaki, A.; Kato, K.; Nagata, F. Development of paclitaxel-loaded poly(lactic acid)/hydroxyapatite core-shell nanoparticles as a stimuli-responsive drug delivery system. *R. Soc. Open Sci.* **2021**, *8*. [[CrossRef](#)]
33. Sato, K.; Kogure, T.; Kumagai, Y.; Tanaka, J. Crystal Orientation of Hydroxyapatite Induced by Ordered Carboxyl Groups. *J. Colloid Interface Sci.* **2001**, *240*, 133–138. [[CrossRef](#)] [[PubMed](#)]
34. Tanizawa, Y.; Sawamura, K.; Suzuki, T. Inhibition of hydroxyapatite formation and growth by condensed phosphate. *Chem. Soc. Jpn.* **1989**, *1989*, 1706–1711. [[CrossRef](#)]
35. Rehman, I.; Bonfield, W. Characterization of hydroxyapatite and carbonated apatite by photo acoustic FTIR spectroscopy. *J. Mater. Sci. Mater. Med.* **1997**, *8*, 1–4. [[CrossRef](#)] [[PubMed](#)]
36. Maçon, A.L.B.; Lee, S.; Poologasundarampillai, G.; Kasuga, T.; Jones, J.R. Synthesis and dissolution behaviour of CaO/SrO-containing sol-gel-derived 58S glasses. *J. Mater. Sci.* **2017**, *52*, 8858–8870. [[CrossRef](#)]
37. Lee, S.; Nakano, T.; Kasuga, T. Structure, dissolution behavior, cytocompatibility, and antibacterial activity of silver-containing calcium phosphate invert glasses. *J. Biomed. Mater. Res. A* **2017**, *105*, 3127–3135. [[CrossRef](#)] [[PubMed](#)]
38. Kister, G.; Cassanas, G.; Vert, M. Effects of morphology, conformation and configuration on the IR and Raman spectra of various poly(lactic acid)s. *Polymer* **1998**, *39*, 267–273. [[CrossRef](#)]
39. Breton, J.; Burie, J.R.; Berthomieu, C.; Berger, G.; Nabedryk, E. The binding sites of quinones in photosynthetic bacterial reaction centers investigated by light-induced FTIR difference spectroscopy: Assignment of the QA vibrations in Rhodobacter sphaeroides using 18O- or 13C-labeled ubiquinone and vitamin K1. *Biochemistry* **1994**, *33*, 4953–4965. [[CrossRef](#)] [[PubMed](#)]
40. Kokubo, T.; Kushitani, H.; Sakka, S.; Kitsugi, T.; Yamamuro, T. Solutions able to reproduce in vivo surface-structure changes in bioactive glass-ceramic A-W. *J. Biomed. Mater. Res.* **1990**, *24*, 721–734. [[CrossRef](#)] [[PubMed](#)]
41. Kuśnieruk, S.; Wojnarowicz, J.; Chodara, A.; Chudoba, T.; Gierlotka, S.; Lojkowski, W. Influence of hydrothermal synthesis parameters on the properties of hydroxyapatite nanoparticles. *Beilstein J. Nanotechnol.* **2016**, *7*, 1586–1601. [[CrossRef](#)] [[PubMed](#)]
42. Wang, S.-B.; Chen, A.-Z.; Weng, L.-J.; Chen, M.-Y.; Xie, X.-L. Effect of Drug-loading Methods on Drug Load, Encapsulation Efficiency and Release Properties of Alginate/Poly-L-Arginine/Chitosan Ternary Complex Microcapsules. *Macromol. Biosci.* **2004**, *4*, 27–30. [[CrossRef](#)]
43. El-Say, K.M. Maximizing the encapsulation efficiency and the bioavailability of controlled-release cetirizine microspheres using Draper-Lin small composite design. *Drug Des. Dev. Ther.* **2016**, *10*. [[CrossRef](#)] [[PubMed](#)]
44. Al-Amin, M.D.; Bellato, F.; Mastrotto, F.; Garofalo, M.; Malfanti, A.; Salmaso, S.; Caliceti, P. Dexamethasone Loaded Liposomes by Thin-Film Hydration and Microfluidic Procedures: Formulation Challenges. *Int. J. Mol. Sci.* **2020**, *21*, 1611. [[CrossRef](#)] [[PubMed](#)]

-
45. Brown, W.E.; Patel, P.R.; Chow, L.C. Formation of CaHPO₄·2H₂O from Enamel Mineral and Its Relationship to Caries Mechanism. *J. Dent. Res.* **1975**, *54*, 475–481. [[CrossRef](#)] [[PubMed](#)]
 46. Juhász, Á.; Ungor, D.; Berta, K.; Seres, L.; Csapó, E. Spreadsheet-based nonlinear analysis of in vitro release properties of a model drug from colloidal carriers. *J. Mol. Liq.* **2021**, *328*, 115405. [[CrossRef](#)]